# Towards patient-specific risk assessment of abdominal aortic aneurysm

Med Biol Eng Comput (2008) 46:1085–1095
DOI 10.1007/s11517-008-0393-0

SPECIAL ISSUE - REVIEW

# Towards patient-specific risk assessment of abdominal aortic aneurysm

**M. Breeuwer · S. de Putter · U. Kose · L. Speelman · K. Visser · F. Gerritsen · R. Hoogeveen · R. Krams · H. van den Bosch · J. Buth · T. Gunther · B. Wolters · E. van Dam · F. van de Vosse**

Received: 27 September 2006 / Accepted: 1 September 2008 / Published online: 23 September 2008


**Abstract** Diagnosis of vascular disease and selection and planning of therapy are to a large extent based on the geometry of the diseased vessel. Treatment of a particular vascular disease is usually considered if the geometrical parameter that characterizes the severity of the disease, e.g. % vessel narrowing, exceeds a threshold. The thresholds that are used in clinical practice are based on epidemiological knowledge, which has been obtained by clinical studies including large numbers of patients. They may apply "on average", but they can be sub-optimal for individual patients. To realize more patient-specific treatment decision criteria, more detailed knowledge may be required about the vascular hemodynamics, i.e. the blood flow and pressure in the diseased vessel and the biomechanical reaction of the vessel wall to this flow and pressure. Over the last decade, a substantial number of publications have appeared on hemodynamic modeling. Some studies have provided first evidence that this modeling may indeed be used to support therapeutic decisions. The goal of the research reported in this paper is to go one step further, namely to investigate the feasibility of a patient-specific hemodynamic modeling methodology that is not only effective (improves therapeutic decisions), but that is also efficient (easy to use, fast, as much as possible automatic) and robust (insensitive to variation in the quality of the input data, same outcome for different users). A review is presented of our research performed during the last 5 years and the results that were achieved. This research focused on the risk assessment for one particular disease, namely abdominal aortic aneurysm, a life-threatening dilatation of the abdominal aorta.

**Keywords** Hemodynamics · Vascular disease · Abdominal aortic aneurysm · Flow modeling · Biomechanical stress modeling · Patient specificity

M. Breeuwer (✉) · U. Kose · K. Visser · F. Gerritsen
Philips Healthcare, Healthcare Informatics, Building QV 162,
P.O. Box 10.000, 5680 DA Best, The Netherlands
e-mail: Marcel.Breeuwer@philips.com

S. de Putter · L. Speelman · F. Gerritsen · T. Gunther · B. Wolters · E. van Dam · F. van de Vosse
Faculty of Biomedical Engineering,
Eindhoven University of Technology, P.O. Box 512,
5600 MB Eindhoven, The Netherlands

R. Hoogeveen
Philips Healthcare, Magnetic Resonance Imaging,
P.O. Box 10.000, 5680 DA Best, The Netherlands

R. Krams
Department of Bioengineering, Imperial College London,
South Kensington Campus, London SW7 2A2, UK

H. van den Bosch
Department of Radiology, Catharina Hospital Eindhoven,
Michelangelolaan 2, 5623 EJ Eindhoven, The Netherlands

J. Buth
Department of Vascular Surgery, Catharina Hospital Eindhoven,
Michelangelolaan 2, 5623 EJ Eindhoven, The Netherlands

## 1 Introduction

Diagnosis of vascular disease and selection and planning of therapy are to a large extent based on the geometry of the diseased vessel. For example, a stenosis (narrowing) of a blood vessel is usually quantified by relating the lumen (blood) diameter or cross-sectional area at the location of the stenosis to the lumen diameter/area at a reference location without stenosis [1]. Similarly, a vascular aneurysm (dilatation) is characterized primarily by its diameter

[37]. Treatment of a particular vascular disease is usually considered if the geometrical parameter that characterizes the severity of the disease exceeds a threshold. For example, patients with coronary-artery stenosis become eligible for treatment if the percentage stenosis exceeds 50% [41]. Similarly, surgical repair of an abdominal aorta aneurysm (AAA), a life-threatening dilatation of the abdominal aorta, is usually performed if its diameter exceeds 55 mm [14, 25].

The thresholds that are used to decide whether or not an AAA should be treated are based on epidemiological knowledge, which has been obtained by clinical studies including large numbers of patients [38]. They may apply "on average", but they can be sub-optimal for individual patients. An AAA is usually not treated if its diameter is less than 55 mm. However, about 15% of the AAA patients experience rupture before the diameter reaches 55 mm [25]. Also, a significant percentage of AAA patients that cannot be treated experience growth to diameters as large as 80 mm, without any rupture. Several studies have confirmed that the AAA diameter is not reliable as patient-specific rupture-risk criterion [8, 22, 47].

To realize patient-specific treatment criteria, more detailed knowledge may be required about the dynamic blood flow (velocity) and pressure in the diseased vessel and about the biomechanical reaction of the vessel wall to this flow and pressure. With existing technology, these quantities cannot be accurately measured at every location in the vessel. Estimation of these quantities may however be possible thanks to recent advances in the field of medical imaging [13], image processing [52] and hemodynamic modeling [26].

Several recent studies have provided first evidence that knowledge of hemodynamic parameters, especially of the vessel-wall stress, may indeed be valuable to enhance therapeutic decisions [10, 11, 33, 45, 46]. For example, in [10] the difference in peak wall stress between patients with electively repaired AAAs and patients with symptomatic or ruptured AAAs was studied. It was found that peak wall stresses were significantly higher for the latter group. In [45] it was concluded that the AAA wall stress at maximum systolic blood pressure is significantly higher for ruptured than for asymptomatic aneurysms.

The goal of the research reported in this paper is to investigate the feasibility of a patient-specific hemodynamic modeling methodology that is not only effective (improves therapeutic decisions), but that is also efficient (easy to use, fast, as much as possible automatic) and robust (insensitive to variation in the quality of the input data, same outcome for different users). We review our recent investigations into automated patient-specific AAA rupture-risk prediction on the basis of hemodynamic modeling and we summarize our results.

## 2 Methods

### 2.1 The hemodynamic modeling chain

Figure 1 depicts the steps involved in patient-specific hemodynamic modeling of AAA.

The first step is the *imaging* of the diseased vessel. Three-dimensional (3D) imaging is required, since the flow and wall-stress modeling require information about the 3D geometry of the vessel. This can currently be performed with computed tomography (CT) and magnetic resonance (MR) imaging. Furthermore, the blood flow velocity that is needed as boundary condition for the flow modeling (at the inlet of the vessel) can be obtained with Quantitative MR Flow imaging (Qflow).

The next step is the derivation of the patient-specific geometry of the various components of the diseased vessel. These components may include the lumen (blood), wall, thrombus (blood clotted against the wall) and calcifications located inside the wall. The automatic derivation of the geometry of these vessel components is henceforth referred to as *segmentation*.

Hemodynamic modeling is usually performed by means of computer simulation on powerful computers, using finite-element or finite-volume calculation techniques. These techniques require a 3D discretisation (*volume meshing*) of the vessel geometry as input.

The raw output of the computer simulations consists of approximations of the physical unknowns (flow velocity, pressure) in every volume mesh node. Intuitive yet comprehensive *visualization* of this abundance of data is essential for clinical interpretation.

### 2.2 Imaging

In patients with diagnosed AAA, the diameter of abdominal aorta aneurysms is usually monitored once or twice a year with 2D ultrasound (US) imaging. Prior to surgical repair, 3D contrast-enhanced CT angiography (CTA) is conventionally used to assess the AAA geometry and to plan the most appropriate repair procedure. In this paper, we report on the application of conventional non-cardiac-triggered 3D contrast-enhanced CTA as well as innovative cardiac-triggered 2D and 3D magnetic resonance imaging (MRI) without breath holding [5].

The use of MRI for AAA imaging is relatively new. A major advantage of MRI compared with CTA is the lack of harmful radiation. An important additional advantage is its enormous flexibility. By adapting scanner settings, different aspects of the vessel can be dynamically visualized, such as lumen, thrombus, wall or blood flow. Table 1 lists the particular settings (often called pulse sequences) applied in our investigations together with their primary aim. It should be noted that no contrast agents are required for any of these

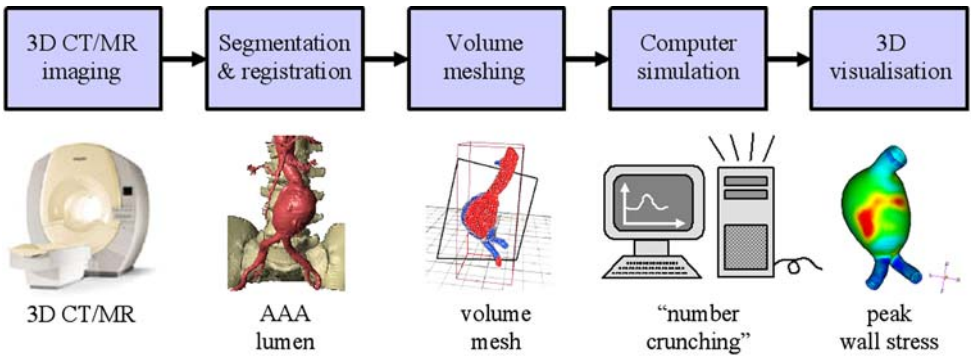


**Fig. 1** The patient-specific hemodynamic modeling chain

sequences. Disadvantages of the use of our MRI pulse sequences are the somewhat lower imaging resolution than CTA, the significantly longer scanning time and the inability to accurately visualize calcifications in the vessel wall.

A total of 30 AAA patients were scanned at the Catharina Hospital Eindhoven with CTA and MRI. Figure 2 shows examples of acquired images for one of the patients.

### 2.3 Segmentation

Manual delineation of the AAA geometry in 3D CT and MR images is a very tedious, time-consuming activity that leads to great variability in the geometry created by different users [10, 15, 46]. As a consequence, also the simulated flow and wall-stress values may vary greatly. For, example in [15] an inter-user variation was found of over 100% between the lowest and highest stress value for the same patient (manual segmentation of CTA image data). Automation of the contour delineation may help to reduce user-induced stress variability [33, 45].

As can be seen in Fig. 2, neither CTA nor MRI can clearly discriminate the AAA wall from thrombus. Our segmentation research has therefore focused on finding the lumen-thrombus boundary and on finding the location of the outer wall. An almost-automatic segmentation technique has been developed that consists of the following steps (Fig. 3).

The first step is the semi-automatic tracking of the lumen centerline (Fig. 3a). The user manually specifies a start point inside the lumen, just below the renal arteries and two end points a few cm below the bifurcation in each of the legs (for CTA). The resolution of MRI does not yet allow accurate segmentation of the bifurcation, therefore only one end point is specified just above the bifurcation. Automatic vessel tracking [50] is used to automatically find the centerline from start to end point(s). For CTA, the two tracked centerlines are merged into one if their distance is closer than a user-selectable threshold (few mm).

The next step is the automatic lumen segmentation. A tube-like initial 3D active object (3DAO), a simplex-mesh-based deformable model [12], is created around the detected centerline (Fig. 3b). This 3DAO is automatically deformed towards the lumen-thrombus boundary or to the lumen-inner wall boundary if thrombus is absent (Fig. 3c). A so-called "external force" derived from image features drives the 3DAO towards the desired boundary, whereas an "internal force" depending on the 3DAO surface curvature

**Table 1** MR pulse sequences used for AAA imaging

| Sequence | Slice distance / thickness (mm) | Pixel spacing (mm x mm) | TE (ms) / TR (ms) / Flip angle (degree) | Coverage / Aim |
|---|---|---|---|---|
| 3D Steady-State Free Precession (SSFP) MRI | 3 / 6 | 0.59 x 0.59 | 6.3 / 1.9 / 50.0 | 40-50 slices (3D), 20-25 slices (M2D), 10-15 phases, from a few cm above AAA to a few cm after the bifurcation into the legs / imaging of the lumen and thrombus/wall |
| Multiple 2D (M2D) SSFP MRI | 6 / 6 | 0.59 x 0.59 | 6.3 / 1.9 / 50.0 | |
| Quantitative Flow (Qflow) MRI | Variable / 6 | 0.43 x 0.43 | 7.6 / 4.1 / 8.0 | 1 slice above the AAA (inflow), 1 slice in each of the bifurcations (outflow), 3-5 slices through the AAA (for validation) (15-20 phases) / quantitative imaging of the blood flow velocity perpendicular to the scan plane |

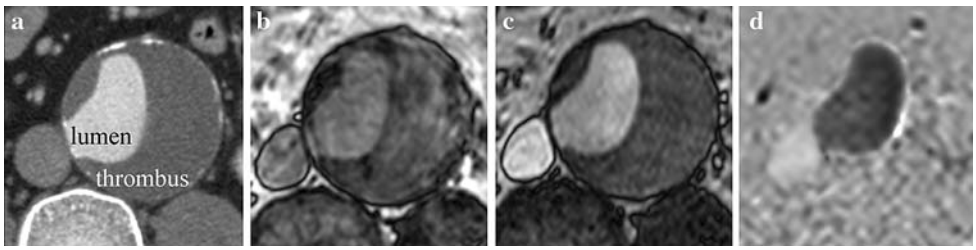


**Fig. 2** Examples of CTA/MR images of 1 AAA patient: **a** CTA, **b** 3D SSFP MRI, **c** 2D SSFP MRI, **d** Qflow MRI (1 transversal slice is shown)

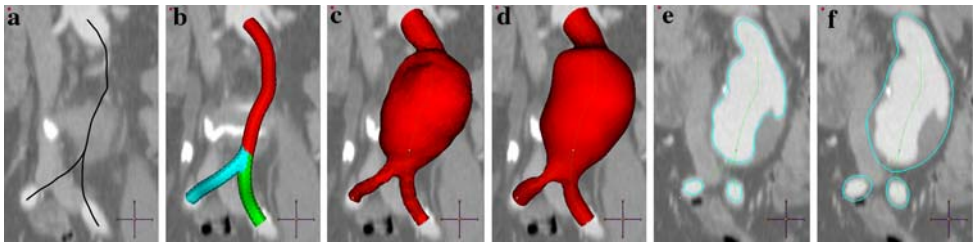


**Fig. 3** Illustration of CTA segmentation: **a** initial centerline, **b** tube around the centerline, **c** segmented lumen, **d** segmented outer wall, **e** sagittal cut through lumen segmentation, **f** sagittal cut through outer wall segmentation

and mesh vertices distribution ensures the smoothness and regularity of the 3DAO [12, 23]. For CTA, the image intensity itself is used as feature; the deformation is terminated at the transition from the expected lumen intensity (Hounsfield value) to the expected thrombus or wall intensity [23]. For MRI, first an edge feature image is created and the deformation is terminated at the position of the lumen-thrombus or lumen-inner wall edge [28].

The final step is the segmentation of the AAA outer wall by deforming the earlier segmented lumen 3DAO towards the AAA outer wall boundary (Fig. 3d). For CTA, this is performed with a technique reported in [23]. Basically, intensity profiles are sampled along the lumen 3DAO surface normal and these profiles are classified using k-nearest neighbor classification, where the possible classes were derived in a training phase from a set of representative intensity profiles. The external force is then derived from the profile classification. For MRI, the outer wall segmentation is performed using the dark intensity ring that is present in the 2D SSFP image around the AAA as image feature. The external force attracts the 3DAO towards this dark ring [28].

The segmentation of the Qflow MR images is performed with a technique similar to that used in the Philips View-Forum Cardiac MR Analysis software product [4]. The Qflow MR amplitude images are used to semi-automatically detect the lumen boundary (Fig. 4, top row). The user only has to manually specify one lumen contour in the image that was acquired at the end-diastolic phase (time moment); this contour is then automatically propagated to all other phases in the cardiac cycle. The blood flow velocity profile, i.e. the velocity as a function of the position inside the segmented lumen contour and as function of the time in the cardiac cycle, is then measured from the Qflow MR phase-contrast (velocity) images (Fig. 4, bottom row).

The flow velocity profile that was measured by MRI is used as inflow boundary condition for the AAA blood flow simulations, both for 3D CTA and MRI. Rigid image registration between CTA and 3D SSFP MRI images is used to relate the CTA and MRI scanning geometries (Fig. 5) [17]. It has been assumed that the 3D SSFP and Qflow MR images are well aligned, since they are recorded during the same MRI examination. The derived rigid image transformation can then be used to map the lumen contour and the measured flow to the location of the lumen in the CTA images. Manual correction of the lumen contour is possible if the alignment is imperfect.

### 2.4 Volume meshing

Two volume-meshing approaches have been implemented: hexahedral meshing by deformation of a standard mesh [51] and Delauney tetrahedral meshing [29]. Hexahedral meshes are particularly suited for finite-element/volume calculations, but they are less suited for accurately representing complex highly curved geometries. Furthermore, deformation of a standard mesh may lead to degenerated hexahedral elements. Tetrahedral meshes can accurately represent complex geometries, but they are generally less optimal for finite-element/volume calculations (more elements, higher calculation times needed to achieve the same accuracy as with hexahedral meshes) [2]. In our experiments, we have chosen the number of hexahedral and tetrahedral elements such that as much as possible similar simulation accuracies were obtained.

### 2.5 Computer simulations

#### *2.5.1 Flow simulations*

Flow models based on the Navier–Stokes equations have been used for the flow simulations. A study has been performed into the benefit of using the patient-specific blood

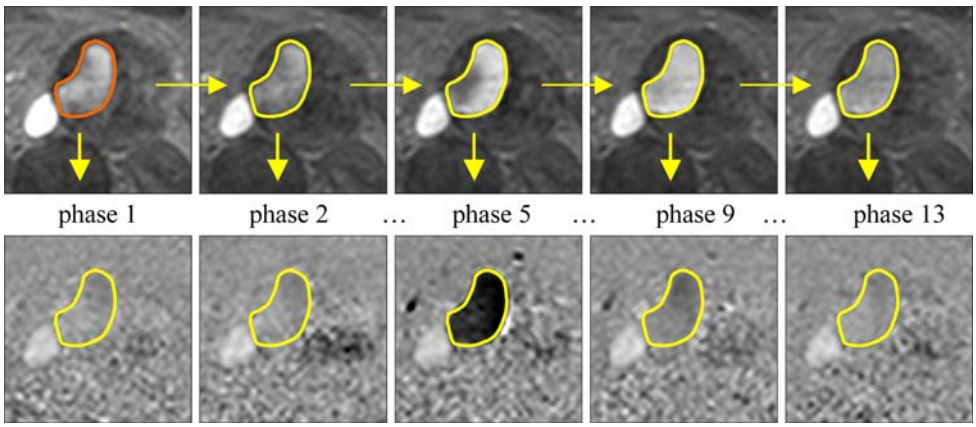


**Fig. 4** Qflow MRI segmentation procedure: the user draws a contour on phase 1 of the Qflow amplitude image. This contour is propagated to all other phases of the amplitude image and can be manually adjusted, if needed. Thereafter the contours are copied to the Qflow phase-contrast images. For every pixel inside the contour the flow velocity is derived from the image intensity in the phase-contrast Qflow image (see [45])

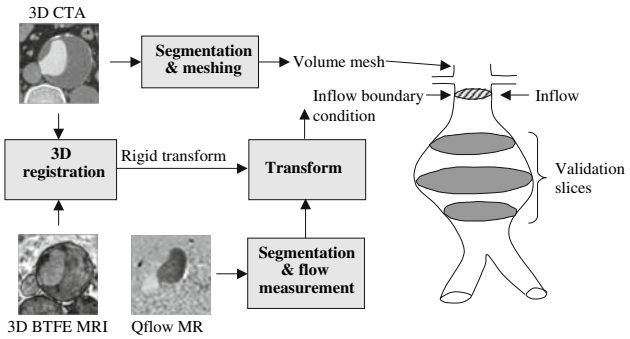


**Fig. 5** Creation of the inflow boundary conditions; location of validation slices

inflow velocity profile measured with Qflow MRI as boundary condition for the flow simulations [17]. The outcome of the flow simulations was compared to the flow velocity profile measured with Qflow MRI at a number of locations around the middle of the AAA (the validation slices in Fig. 5). The results were also compared to those obtained when using the conventionally used plug-flow input profile. All flow simulations were performed with the CFD-ACE + finite-volume simulation package from the ESI Group.

### 2.5.2 *Wall stress simulations*

The wall stress simulations were performed assuming a neo-Hookean model describing an isotropic linearly elastic medium with large deformations. Since no information about the wall thickness and wall material properties could be derived from the CTA or MR images, a homogeneous wall of constant thickness of 2 mm was assumed with a shear modulus of 1.0 MPa. All simulations were performed with the Sepran finite-element simulation package (Sepra, Delft, The Netherlands).

With existing imaging technology the in vivo measurement of the stress in a vessel wall is impossible. No ground truth was thus available to determine the accuracy of the wall stress simulations. The investigations have therefore focused on analyzing the sensitivity of the simulations to variations in the AAA geometry, on studying the potential influence of calcifications in the AAA wall and on properly handling the patient's blood pressure as boundary condition for the simulations. Three separate studies were performed, which will be described below. An evaluation into the clinical value of wall-stress (and flow) modeling is ongoing (see Sect. 5).

In wall-stress study I, the sensitivity of the wall-stress simulations with respect to geometrical variations was investigated, using MR and CTA images from four patients with AAA [30]. The geometry of the AAA outer wall was automatically segmented as well as twice manually delineated by three individual users. The influences of the volume mesh resolution, the automatic and manual contour segmentation variability, and the difference between CTA or MR images on the simulated wall stress were measured.

In study II the influence of the presence of calcifications in the AAA wall on the wall stress was investigated [31]. The material properties reported in literature for calcifications and the material properties actually used for simulations show great variation. Previous studies have focused on simplified modeling of the calcification shapes within a realistic aneurysm shape [20, 42]. In our study, an accurate representation of the calcification geometry and a simplified model for the AAA were used. The objective of this approach was to investigate to what extent the calculated wall stress depends on the calcification geometry, the material properties and the modeling approach. For four realistic calcification shapes segmented from clinical CTA AAA images, simulations were performed with three distinct modeling approaches, at five distinct elasticity settings. Figure 6 shows the four calcification geometries used in the study.

Finally, in study III an alternative was evaluated for the commonly used approach of applying the full systolic (highest) blood pressure directly on the aneurysm geometry as it appears in the medical images [32]. Since this approach does not account for the fact that the measured geometry is already experiencing a substantial load, it may lead to an

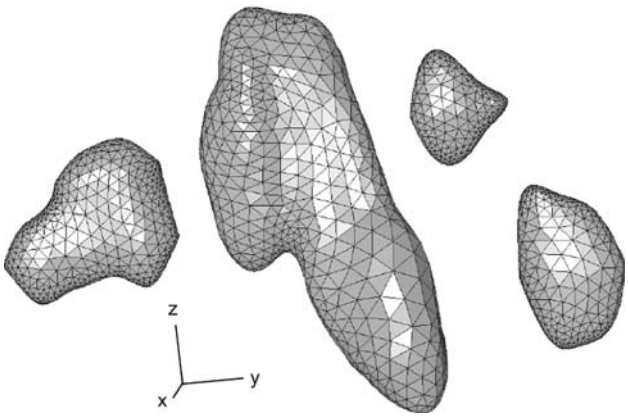


**Fig. 6** Four calcification geometries used in study II

incorrect systolic aneurysm shape and therefore to incorrect wall stress values. A method was developed to compute the wall stress at any given pressure above the diastolic (lowest) pressure, starting from the true diastolic geometry. The method has the advantage over earlier-proposed methods [19, 34] that it does not require any modification of the finite-element solution methods. The effect of incorporating the initial diastolic stress into the AAA wall stress simulations was assessed for three patient-specific AAA geometries acquired with cardiac-triggered MRI.

### 2.6 Visualization

The flow and wall-stress simulations result in an enormous amount of data that must be intuitively and comprehensively presented to the clinical user. To achieve this we have built a dedicated flow-velocity (and derived parameters such as wall shear stress) and wall-stress visualization software package [16] on top of the publicly available Visualization Toolkit (VTK) software library [35]. With this dedicated package it is possible to visualize the relation between flow/stress and the vessel geometry, to show the relation between the segmented vessel and the surrounding anatomy and to show movies of the flow/stress variation over time.

## 3 Results

### 3.1 Flow modeling

We found that the AAA lumen can be clearly visualized with CTA as well as with MRI, especially with 2D SSFP MRI. For all patients that were studied so far, the lumen surface could be successfully semi-automatically segmented from the CTA data (including the bifurcation into the legs) [23] and from the MRI data (up to the bifurcation) [17]. The agreement between automatic and manual segmentations is comparable to values reported in the literature, whereas the required user interaction is minimal (mean segmentation error below 1.0 mm) [27].

The blood velocity inflow profiles that were derived from Qflow MRI could be successfully registered to the correct locations in the CTA image data, although manual corrections were sometimes needed [17]. Tetrahedral and hexahedral volume meshes could be automatically generated based on the obtained lumen surface segmentations [29, 51]. Overall time needed for lumen segmentation, derivation of the Qflow profile, registration and meshing was less than 5 min per image data set on a Dell 650, Dual Processor, 3 GHz PC (including time needed for manual corrections).

In our flow simulations, a greater correlation between the measured and the simulated flow was found when using the patient-specific inflow profile than when using a plug-flow shaped inflow profile, both with a patient-specific flux value (average correlation coefficient 0.75 for patient-specific inflow profile, 0.67 for plug-flow profile) [17]. Figure 7 shows an example of the measured and simulated flux for one of the AAA geometries.

### 3.2 Wall-stress modeling

Automatic segmentation of the outer wall from CTA data proved to be feasible, although manual corrections were regularly needed at locations where the difference in intensity of the AAA wall and surrounding tissue was relatively small. In an evaluation using 17 CTA data sets a mean segmentation error of 1.3 mm (SD 0.4 mm) was found [23].

Automatic segmentation of the AAA outer wall on the basis of 2D/3D SSFP MRI data appeared to be feasible with an accuracy comparable to what has been reported in literature for CTA (four MR data sets, mean segmentation error below 1 mm) [23, 27, 28, 49]. The resolution of the

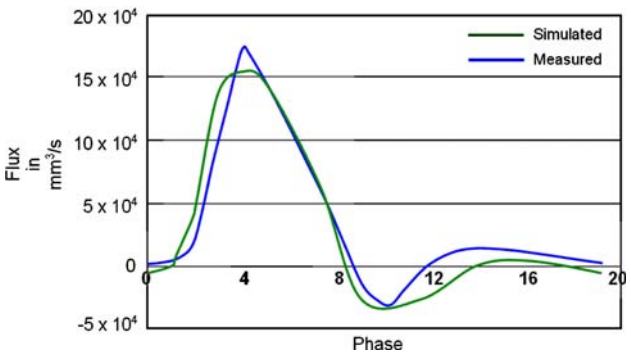


**Fig. 7** Measured versus simulated flux for one AAA geometry

MRI data was too low to allow segmentation of the outer wall below the bifurcation into the legs.

Neither CTA nor MRI could provide accurate information on the location of the AAA inner wall. Consequently, no information about the wall thickness could be derived. Furthermore, no information about the wall material properties could be obtained by imaging alone. An exception may be the presence of calcifications; in the CTA data these are clearly visible as bright spots near the AAA outer wall. The stiffness of the calcifications could however not be obtained via imaging. In our MRI data, calcifications were not clearly visible. As mentioned before, rigid registration of 3D CTA and 3D SSFP MRI data seems to be feasible. More locally optimized non-rigid registration may however be needed to accurately map calcifications detected in the CTA data to the outer wall segmentation derived from the MRI data.

So far, we only used volume meshing assuming a wall of constant thickness. High-quality meshes, suited for wall stress simulation could be automatically generated in all cases that we studied. Overall time needed for outer wall segmentation and meshing was less than 5 min per image data set on a Dell 650, Dual Processor, 3 GHz PC (including time needed for manual corrections).

Study I on the sensitivity of the wall-stress calculations for geometrical variation in the AAA outer wall segmentation showed that the peak wall stress is reproducible for most of the studied AAA geometries [30]. The 0.99 percentiles of the wall stress show excellent reproducibility for all studied AAAs (less than 6% variation when using repeated automatic segmentation with different manual initializations). The wall-stress variations induced by fully manual contour drawing are much larger than those caused by the automatic segmentation variability (repeated manual contours drawing resulted in 20% variation in the 0.99 percentile of the wall stress for CTA and 18% for MRI). The influence of the user variability appears to be similar for MR and CT. As an example, Fig. 8 shows the von Mises wall stress based on the manual MRI segmentations. The differences in the value and location of the maximum (of the von Mises) stress can be clearly observed.

Study II on the influence of calcifications has supplied insight into how sensitive the peak wall stress is to variation in the elasticity of the calcifications. For relatively elastic calcifications, the results from the various modeling approaches that were studied agree and the computed wall stress in the tissue surrounding the calcifications shows to be insensitive to the exact calcification geometry [31]. For stiffer calcifications, however, the different modeling approaches and the different geometries lead to significantly different results. A recent study confirmed that calcifications can significantly influence the local wall stress [43]. This indicates the importance of further study into methods for accurately determining and modeling the vessel wall material properties. Figure 9 illustrates the differences in the wall stress induced by elastic and stiff calcifications. It can clearly be seen that a stiff calcification induces much larger local stress values.

Study III into the effect of taking the initial blood pressure load at end diastole into account shows that this approach performs better than the conventionally used approach of applying the full systolic blood pressure to the end-diastolic AAA geometry [32]. We found that the conventional approach leads to an unrealistically smooth systolic geometry and therefore to an underestimation of the systolic peak wall stress of up to 28%. Our new "initial-load" approach overcomes these issues and provides a more plausible estimate for the systolic aneurysm volume and a significantly different estimate for the peak wall stress.

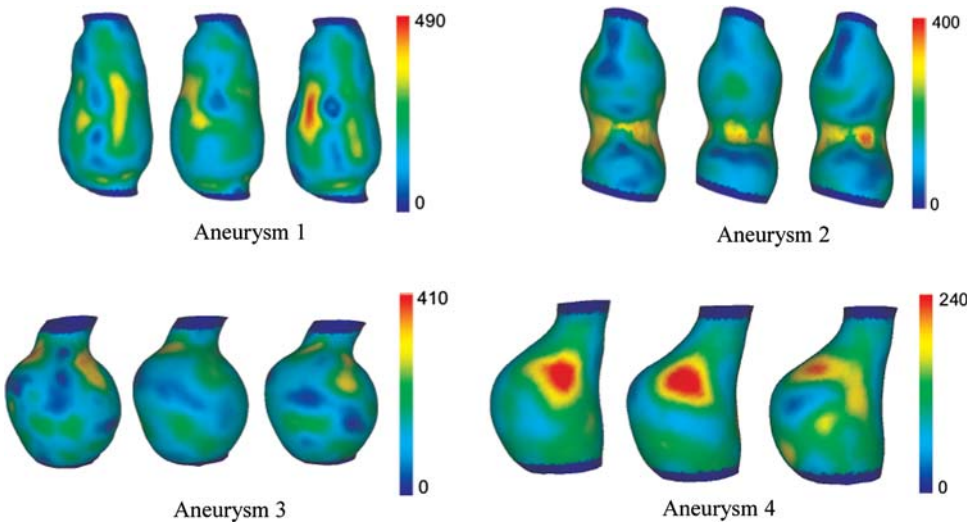


**Fig. 8** The von Mises wall stress (kPa) based on the three manual MRI segmentations

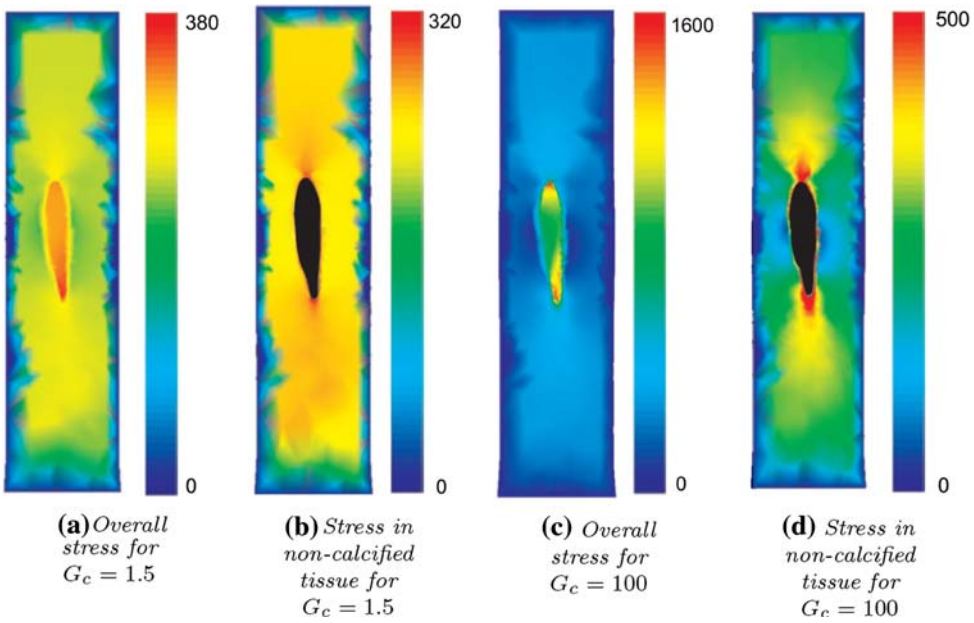


**Fig. 9** Differences in von Mises wall stress (kPa) induced by elastic (shear modulus $G_c = 1.5$) and stiff calcifications ($G_c = 100$). In **a** and **c** the stress in the calcification and the surrounding tissue are shown, in **b** and **d** only the stress in the surrounding tissue is displayed

## 4 Discussion

To realize true patient-specific hemodynamic modeling, patient-specific information is required about the geometry of the various vessel components, about the material properties of each of these components and about the blood inflow velocity and the blood pressure at the in- and outflow boundaries. Furthermore, computational fluid and mechanical models are needed that realistically describe the behavior of the blood and the various tissue components.

In the research performed during the last few years, we have been able to reach a fairly high level of patient specificity. However, important information that is required for true patient-specific modeling is still missing. Table 2 briefly summarizes the required patient-specific information and the extent to which it could be obtained with the imaging protocols and approaches used in our study.

The lumen geometry and blood inflow profile were successfully used for blood flow simulations. A good agreement was found between the simulated and the measured blood flow velocities inside the AAA (Fig. 7). So far,

**Table 2** Extent to which required patient-specific information can be acquired

| **Geometry** | **Available?** |
|---|---|
| lumen | yes, via 3D CTA or 2D/3D BTFE MRI |
| thrombus | only the lumen-thrombus transition via 3D CTA or 2D/3D BTFE MRI, not the thrombus-wall transition |
| wall | only the outer wall via 3D CTA or 2D/3D BTFE MRI, not the wall-thrombus transition; the exact wall thickness is therefore not known |
| calcifications | yes, via 3D CTA |
| **Boundary conditions** | **Available?** |
| blood flow velocity | inflow velocity can be obtained with Qflow MRI, 3D BTFE MRI can be used to map the flow data to CTA |
| blood pressure | only roughly via external measurement |
| **Material properties** | **Available?** |
| all materials | not with the imaging protocols used so far, although 2D/3D SSFP MRI shows significant intensity detail in the thrombus |

however, only the velocity component perpendicular to the MR scan plane has been measured. Using the real 3D inflow velocity may increase the accuracy of the flow simulations. Furthermore, in our simulations the lumen geometry was assumed to be rigid, whereas in reality it varies with the pulsating blood pressure. Taking this variation into account may further increase the accuracy. We were able to segment the varying lumen geometry from the 3D SSFP image data [28], but so far we have not used it in our flow simulations. Finally, the use of more realistic constitutive models for blood may also increase the accuracy of the simulations.

We have successfully used the patient-specific AAA outer wall geometry that was automatically derived from CTA and MRI data as input for our wall-stress simulations. Furthermore, on the basis of the dynamic SSFP MRI data, we have been able to derive realistic pressure boundary conditions for our wall stress simulations (taking into account the initial-load at end diastole). However, information about the patient-specific wall thickness and wall material properties are still lacking, since CTA or MRI can presently not obtain these. Therefore, a wall of constant thickness with material properties as reported in literature was used. This will of course significantly limit the patient specificity of our simulations. In [44], for example, it was shown that a wall thickness increase from 1.31 to 1.58 mm results in an increase in stress of up to 21%.

In our wall-stress simulations we have neglected the presence of thrombus. Intraluminal thrombus has been incorporated in the finite-element models in several other studies [9, 21, 48]. In [48] and [9] a significant influence was reported of thrombus on the outcome of the stress calculations. However, very recently [7] and [3] reported extensive studies on the material properties of thrombus. The mean thrombus shear modulus that they found ($1.7 \pm 1.3$ kPa) is much lower than the values assumed in [9, 48], the role of thrombus in wall-stress analysis may therefore be overestimated. The elasticity of thrombus is several orders higher than that of the vessel wall [6], which may mean that thrombus could be neglected during the wall-stress simulations. This corresponds to what has been reported earlier in [36].

Our preliminary experiments into the influence of calcifications in the AAA wall have shown that very stiff calcifications may significantly increase the wall stress. In [31] it is argued that the incorporation of calcifications into the wall stress modeling may be possible simply by locally translating the CTA image intensity to elasticity values used during the simulations (the higher the intensity, the lower the elasticity). A more thorough study is however needed to confirm these first findings.

Although we did measure the patient-specific systolic and diastolic blood pressure during imaging using an external pressure cuff, the peak pressure at the aneurismal site may significantly differ from the peak brachial pressure. It is known however that the human blood pressure varies significantly throughout the day, as a result of varying conditions (stress, anxiety, coffee, sleep, etc.). It is therefore probably more useful to know the patient's blood pressure range than to know the exact pressure during imaging. Both average and worst-case scenarios can then be used during simulation.

In our wall-stress studies, no fluid effects were included in the calculation of the AAA wall stress. To include fluid forces, fluid structure interaction (FSI) models are used in a number of studies [18, 24, 39, 40]. In [18] it was concluded that fully coupled FSI simulation, which requires considerable computational power to run, adds little to rupture-risk prediction. Other studies [24, 40], however, showed influences of up to 25%.

In conclusion, to realize true patient-specific wall-stress modeling, future research should primarily focus on finding methods and models to derive and describe the patient-specific wall thickness and blood, wall- and thrombus material properties.

## 5 Future work

Whether or not the calculated flow and wall-stress values can indeed better predict aneurysm rupture than the currently used aneurysm diameter can only be verified by a clinical evaluation including a sufficiently large number of patients. A preliminary evaluation is currently ongoing in cooperation with the Catharina Hospital Eindhoven and the Academic Hospital Maastricht, The Netherlands. Each hospital will study at least 20 patients with an AAA diameter of more than 4.5 cm and less than 5.5 cm. Each patient will be repeatedly CT and MR imaged at 4-month intervals. The estimated flow and wall-stress values will be correlated with clinically relevant events, such as aneurysm growth, pain symptoms and rupture. Wall models with increasing complexity will be applied (without/with calcifications, without/with initial pressure load, etc.). The study has been approved by the Medical Ethical Committees of the participating hospitals.

We have recently performed a preliminary study in which the simulated aortic wall motion at the location of the AAA was compared with the actual wall motion derived from dynamic MR images. First results show a good correlation, but a more elaborate evaluation is needed to confirm these findings.

## 6 Conclusions

We have reviewed our efforts to realize an accurate, efficient and robust hemodynamic modeling methodology for

assessing the risk of abdominal aorta aneurysm. The approaches that we have developed have a high level of automation and have a fairly high level of patient specificity. More research is however needed to find methods for the assessment of the patient-specific vessel wall thickness and material properties. Furthermore, clinical evaluation of the developed methodologies is needed to determine their true clinical value.

**Acknowledgments** This research was performed in the scope of the Hemodyn project, a cooperation between Philips Healthcare Best (Healthcare Informatics), the Technische Universiteit Eindhoven (Biomedical Engineering department) and the Erasmus University (Thoraxcenter, Biomedical Engineering), Rotterdam, The Netherlands. The Hemodyn project was partly funded by SenterNovem (Dutch Ministry of Economic Affairs). We are grateful to Mustafa Megahed and the CFD Team of the ESI group for the support on interfacing to and using the CFD-ACE+ software.

## References

1. Bartlett ES, Symons SP, Fox AJ (2006) Correlation of carotid stenosis diameter and cross-sectional areas with CT angiography. Am J Neuroradiol 27:638–642
2. Biswas R, Strawn RC (1998) Tetrahedral and hexahedral mesh adaptation for CFD problems. Appl Numer Math 26:135–151
3. Boschetti F, Di Martino E, Gioda G (2007) A poroviscoelastic model of intraluminal thrombus from abdominal aortic aneurysms. Proceedings of the 2007 Summer Bioengineering Conference, Keystone, Colorado, USA
4. Breeuwer M (2005) Quantification of atherosclerotic heart disease with cardiac MRI. MedicaMundi 49(2):30–38
5. Breeuwer M, Götte U, Hoogeveen R, Wolters BJBM, de Putter S, van de Bosch H, Buth J, Rouet J-M, Laffargue F (2004) Assessment of the rupture Risk of abdominal aortic aneurysms by patient-specific hemodynamic modeling—initial results. Int Congr Ser 1268:1090–1095
6. van Dam EV, Dams SD, Peters GWM, Rutten MCM, Schurink GWH, Buth J, van de Vosse FN (2006) Determination of linear viscoelastic behavior of abdominal aortic aneurysm thrombus. Biorheology 43(6):695–707
7. van Dam EA, Dams SD, Peters GW, Rutten MC, Schurink GW, Buth J, van de Vosse FN (2008) Non-linear viscoelastic behavior of abdominal aortic aneurysm thrombus. Biomech Model Mechanobiol 7(2):127–137
8. Darling RC, Messina CR, Brewster DC, Ottinger LW (1977) Autopsy study of unoperated abdominal aortic aneurysms: the case for early resection. Circulation 56(3 Suppl):II161–II164
9. Di Martino E, Mantero S, Inzoli F, Melissano G, Astore D, Chiesa R, Fumero R (1998) Biomechanics of abdominal aortic aneurysm in the presence of endoluminal thrombus: experimental characterisation and structural static computational analysis. Eur J Vasc Endovasc Surg 15(4):290–299
10. Fillinger MF, Raghavan ML, Marra SP, Cronenwett JL, Kennedy FE (2002) In vivo analysis of mechanical wall stress and abdominal aortic aneurysm rupture risk. J Vasc Surg 36(3): 589–597
11. Fillinger MF, Marra SP, Raghavan ML, Kennedy FE (2003) Prediction of rupture risk in abdominal aortic aneurysm during observation: wall stress versus diameter. J Vasc Surg 37(4): 724–732
12. Gerard O, Billon AC, Rouet JM, Jacob M, Fradkin M, Allouche C (2001) Efficient model-based quantification of left ventricular function in 3-D echocardiography. IEEE Trans Med Imaging 21(9):1059–1068
13. Grainger RG, Allison DJ, Adam A, and Dixon AK (eds) (2001) Diagnostic radiology: a textbook of medical imaging. Harcourt Publishers Ltd., London, England. ISBN: 0-443-06432-6
14. Greenhalgh RM, Forbes JF, Fowkes FG, Powel JT, Ruckley CV, Brady AR, Brown LC, Thompson SG (1998) Early elective open surgical repair of small abdominal aortic aneurysms is not recommended: results of the UK small aneurysm trial. Steering committee. Eur J Vasc Endovasc Surg 16(6):462–464
15. Heng MS, Fagan MJ, Collier JW, Desai G, McCollum PT, Chetter IC (2008) Peak wall stress measurement in elective and acute abdominal aortic aneurysms. J Vasc Surg 47(1):17–22
16. Kose U, Visser K, Tryon CL, Breeuwer M (2005) Comprehensive combined visualization of anatomy and hemodynamics. Proc SPIE Med Imaging 5744:435–445
17. Kose U, de Putter S, Hoogeveen R, Breeuwer M (2006) Computational fluid dynamics of abdominal aortic aneurysms with patient-specific inflow boundary conditions. Proc SPIE Med Imaging 6143:61432D1–61432D11
18. Leung JH, Wright AR, Cheshire N, Crane J, Thom SA, Hughes AD, Xu Y (2006) Fluid structure interaction of patient specific abdominal aortic aneurysms: a comparison with solid stress models. Biomed Eng Online 5:33
19. Lu J, Zhou X, Raghavan ML (2007) Inverse elastostatic stress analysis in pre-deformed biological structures: demonstration using abdominal aortic aneurysms. J Biomech 40(3):693–696
20. Marra SP, Chen DT, Fillinger MF, Dwyer JM, Kennedy FE (2005) Effects of including calcified deposits in the finite element modeling of an abdominal aortic aneurysm. Proceedings of the Summer Bioengineering Conference, Colorado, USA
21. Mower WR, Quinones WJ, Gambhir SS (1997) Effect of intraluminal thrombus on abdominal aortic aneurysm wall stress. J Vasc Surg 26(4):602–608
22. Nicholls SC, Gardner JB, Meissner MH, Johansen HK (1998) Rupture in small abdominal aortic aneurysms. J Vasc Surg 28(5):884–888
23. Olabarriaga SD, Rouet JM, Fradkin M, Breeuwer M, Niessen WJ (2005) Segmentation of thrombus in abdominal aortic aneurysms from CTA with nonparametric statistical grey level appearance modeling. IEEE Trans Med Imaging 24(4):477–485
24. Papaharilaou Y, Ekaterinaris JA, Manousaki E, Katsamouris AN (2007) A decoupled fluid structure approach for estimating wall stress in abdominal aortic aneurysms. J Biomech 40(2):367–377
25. United Kingdom Small Aneurysm Trial Participants (2002) Long-term outcomes of immediate repair compared with surveillance of small abdominal aortic aneurysms. N Engl J Med 346(19): 1445–1452
26. Pedley TJ (2003) Mathematical modeling of arterial fluid dynamics. J Eng Math 47:419–444
27. de Putter S (2006) On patient-specific wall stress analysis in abdominal aortic aneurysms. Ph.D. Thesis, 19. ISBN: 90-386-2578-2
28. de Putter S, Breeuwer M, Kose U, Laffargue F, Rouet J-M, Hoogeveen R, van den Bosch H, Buth J, van de Vosse FN, Gerritsen FA (2005) Automatic determination of the dynamic geometry of abdominal aortic aneurysm from MR with application to wall stress simulations. Int Congr Ser 1281:339–344
29. de Putter S, Laffargue F, Breeuwer M, van de Vosse FN, Gerritsen FA (2006) Computational mesh generation for vascular structures. Int J Cars 1:1–11
30. de Putter S, Breeuwer M, van de Vosse F, Kose U, Gerritsen FA (2006) Patient-specific models of wall stress in abdominal aortic

aneurysm: a comparison between MR and CT. Proc SPIE Med Imaging 6143:61430D1–61430D12
31. de Putter S, van de Vosse FN, Breeuwer M, Gerritsen FA (2006) Local influence of calcifications on the wall mechanics of abdominal aortic aneurysm. Proc SPIE Med Imaging 6143:61432E1–61432E11
32. de Putter S, Wolters BJBM, Rutten MCM, Breeuwer M, Gerritsen FA, van de Vosse FN (2007) Patient-specific initial wall stress in abdominal aortic aneurysms with a backward incremental method. J Biomech 40(5):1081–1090
33. Raghavan ML, Fillinger MF, Marra SP, Naegelein BP, Kennedy FE (2005) Automated methodology for determination of stress distribution in human abdominal aortic aneurysm. J Biomech Eng 127(5):868–871
34. Raghavan ML, Ma B, Fillinger MF (2006) Non-invasive determination of zero-pressure geometry of arterial aneurysms. Ann Biomed Eng 34(9):1414–1419
35. Schroeder W, Martin K, Lorensen B (2002) The visualization toolkit, 3rd edn. Kitware, Inc., New York. ISBN: 1-930934-07-6
36. Schurink GWH, van Baalen JM, Visser MJT, van Bockel JH (2000) Thrombus within an aortic aneurysm does not reduce pressure on the aneurysmal wall. J Vasc Surg 31(3):501–506
37. Scott RAP, Wilson NM, Ashton HA, Kay DN (1995) Influence of screening on the incidence of ruptured abdominal aortic aneurysm: 5-year results of a randomized controlled study. Br J Surg 82:1066–1070
38. Scott RA, Ashton HA, Lamparelli MJ, Harris GJ, Stevens JW (1999) A 14-year experience with 6 cm as a criterion for surgical treatment of abdominal aortic aneurysm. Br J Surg 86(10):1317–1321
39. Scotti CM, Shkolnik AD, Muluk SC, Finol EA (2005) Fluid–structure interaction in abdominal aortic aneurysms: effects of asymmetry and wall thickness. Biomed Eng Online 4:64
40. Scotti CM, Jimenez J, Muluk SC, Finol EA (2008) Wall stress and flow dynamics in abdominal aortic aneurysms: finite element analysis vs. fluid–structure interaction. Comput Methods Biomech Biomed Eng 11(3):301–322
41. Smith SC (2001) ACC/AHA guidelines for percutaneous coronary intervention. Circulation 103:3019–3041
42. Speelman L, Bohra A, Makaroun MS, Vorp DA (2005) Assessment of wall calcification in patient-specific finite element analyses of abdominal aortic aneurysm. Proceedings of the Summer Bioengineering Conference, Colorado, USA
43. Speelman L, Bohra A, Bosboom EM, Schurink GW, van de Vosse FN, Makaorun MS, Vorp DA (2007) Effects of wall calcifications in patient-specific wall stress analyses of abdominal aortic aneurysms. J Biomech Eng 129(1):105–109
44. Thubrikar MJ, Al Soudi J, Robicsek F (2001) Wall stress studies of abdominal aortic aneurysm in a clinical model. Ann Vasc Surg 15(3):355–366
45. Truijers M, Pol JA, Schultzekool LJ, van Sterkenburg SM, Fillinger MF, Blankensteijn JD (2007) Wall stress analysis in small asymptomatic, symptomatic and ruptured abdominal aortic aneurysms. Eur J Vasc Endovasc Surg 33(4):401–407
46. Venkatasubramaniam AK, Fagan MJ, Mehta T, Mylankal KJ, Ray B, Kuhan G, Chetter IC, McCollum PT (2004) A comparative study of aortic wall stress using finite element analysis for ruptured and non-ruptured abdominal aortic aneurysms. Eur. J Vasc Endovasc Surg 28(2):168–176
47. Vorp AD, Vande Geest JP (2005) Biomechanical determinants of abdominal aortic aneurysm rupture. Arterioscler Thromb Vasc Biol 25(8):1558–1566
48. Wang DH, Makaroun MS, Webster MW, Vorp DA (2002) Effect of intraluminal thrombus on wall stress in patient-specific models of abdominal aortic aneurysm. J Vasc Surg 36(3):598–604
49. Wever JJ, Blankensteijn JD, van Rijn JC, Broeders IAMJ, Eikelboom BC, Mali WPThM (2000) Inter- and intraobserver variability of CT measurements obtained after endovascular repair of abdominal aortic aneurysms. Am J Roentgenol 175(5):1279–1282
50. Wink O, Frangi AF, Verdonck B, Viergever MA, Niessen WJ (2002) 3D MR coronary axis determination using a minimum cost path approach. Magn Reson Med 47:1169–1175
51. Wolters BJBM, Rutten MCM, Schurink GW, Kose U, de Hart J, van de Vosse FN (2005) A patient-specific computational model of fluid-structure interaction in abdominal aortic aneurysms. Med Eng Phys 27(10):871–883
52. Yoo TS (ed) (2004) Insight into images: principles and practice for segmentation, registration, and image analysis. AK Peters Ltd., Wellesley, MA. ISBN: 1568812175